



Seismic Response Analysis of Underground Granary Under Different Incident Directions

Hao Zhang, Chuang Mu, Lei Chen*

Henan University of Technology, Zhengzhou, Henan, 450001, China

*Corresponding author's e-mail: chenlei@haut.edu.cn

Abstract. To investigate the dynamic response characteristics and patterns of underground grain silos subjected to seismic waves from different incident directions, viscoelastic boundaries were employed to simulate the infinite foundation as a continuously distributed spring-damper system on artificial boundaries. A soil-underground grain silo structural model was developed using ABAQUS, into which horizontal seismic waves, vertical seismic waves, and horizontally-vertically coupled seismic waves were input. The acceleration, displacement, and stress responses of the underground structure were analyzed. The results indicate that the maximum horizontal acceleration of the silo wall under coupled seismic action increases by approximately 6% compared to that under horizontal seismic action alone, and the maximum vertical acceleration of the silo wall under coupled seismic action increases by about 12% compared to that under vertical seismic action alone. Therefore, the silo wall exhibits a more significant response under coupled seismic excitation, with a greater impact on vertical seismic effects. The position of maximum tensile stress occurs at the bottom of the silo wall under horizontal and horizontally-vertically coupled seismic waves, whereas it appears at the top of the silo wall under vertical seismic waves.

Keywords: underground granary, viscoelastic boundary, silo wall, vertical earthquake

1 Introduction

The prevalent issues in grain storage include low land utilization efficiency and high energy consumption for grain preservation^[1]. Underground grain silos, however, effectively reduce the need for ventilation and cooling, eliminate the need for fumigation, inhibit pest infestation, ensure long-term grain quality, achieve green grain storage, and extend the grain storage period. Despite these advantages, underground silos have not been widely promoted and applied^[2]. Grain security is crucial to national economy and people's livelihood, The current diameter of underground grain storage silos has reached 25m, and their waterproof and moisture-proof performance requirements are significantly higher than those of typical underground structures. However, there has been no research conducted on their seismic performance. Therefore, it is necessary to conduct seismic checks and calculations for these structures. Traditionally, under-

ground structures are considered to have better seismic performance than above-ground structures due to the constraint provided by the surrounding soil. However, historical earthquake damages have shown that underground structures can sustain damage during earthquakes, such as the severe damage to the Daikai subway station during the 1995 Kobe earthquake^[3]. Since then, various scholars at home and abroad have conducted research on the seismic performance of underground structures^[4-7]. MZ Xu^[8] established a numerical model considering fluid-solid coupling and different earthquake intensities to explore the impact of varying groundwater levels on the seismic behavior of underground stations. Huang Weizhen^[9] conducted in-depth research on the dynamic response patterns of immersed tunnels and their shear keys under obliquely incident seismic waves, finding that oblique incidence has the greatest impact on the vertical response of tunnels. Gu Kunsheng^[10] studied the dynamic response characteristics of single-sided slopes under the influence of incident angles based on the theory of elastic waves in the time domain and viscoelastic boundary conditions, using window harmonic waves. In the seismic resistance of slender structures, the non-uniformity of ground motions must be considered. ZD Cui^[11] established a two-dimensional finite element model of soil-station based on the Daikai station to explore the failure modes of bearings under different earthquake intensities and introduced the concept of incremental bearing damage to quantitatively analyze the structural damage caused by the main earthquake and subsequent aftershocks. Zhu Hui^[12] converted seismic waves into equivalent node loads on viscoelastic boundaries based on wave theory, established load calculation formulas for SV waves under oblique incidence, and studied the dynamic response characteristics of shallow-buried tunnels under biased pressure. All the above studies have investigated the dynamic response of structures under different incident angles, providing a reference for research on the seismic resistance of underground grain silos under seismic waves from different incident directions

In this paper, a three-dimensional soil-structure model of an underground grain silo is established using ABAQUS. The seismic wave input method is implemented by converting the seismic wave into equivalent node loads on viscoelastic boundaries to facilitate the input of seismic waves. The study investigates the acceleration response, displacement response, and stress response of the underground grain silo wall under different incident directions of seismic waves. The findings provide valuable references for the structural design of underground grain silos and promote their promotion and application.

2 Construction of Finite Element Model of Underground Granary

2.1 Project Overview

Selected for this study is a steel-concrete composite underground grain storage facility, featuring a diameter of 25 meters and a total depth of 24.5 meters. The concrete thickness on the top of the silo measures 250 millimeters, while the steel plate has a

thickness of 6 millimeters. The concrete wall of the silo is 300 millimeters thick, reinforced internally with a steel mesh. Both the circular and vertical reinforcement bars have a diameter of 16 millimeters and are spaced at intervals of 200 millimeters. The steel plate of the silo wall is 10 millimeters thick, and the steel plate at the bottom is 8 millimeters thick. The internal lining steel plates are connected to the concrete through studs, as illustrated in Figure 1. Within a soil exploration depth of 60 meters at the project site, the soil is predominantly silty clay, with a groundwater table buried at a depth of approximately 3.4 to 3.8 meters.

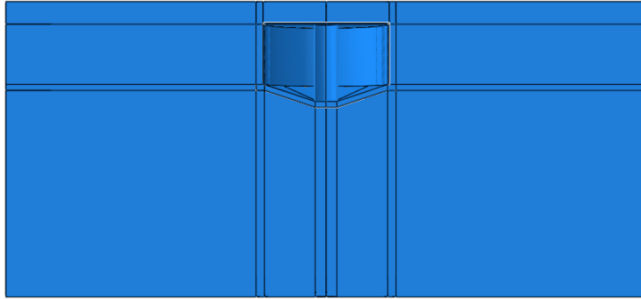


Fig. 1. Soil body-structure diagram.

2.2 Finite Element Model of Underground Granary

Based on an actual engineering project, a finite element model (FEM) of the same-sized underground grain storage facility was established. This study focuses on the overall seismic performance of the silo wall, with relevant components simplified accordingly. The FEM primarily comprises four parts: soil, cast-in-situ concrete, lined steel plates, and reinforcing steel bars.

When analyzing the seismic response of underground structures, the size of the soil domain is a critical consideration. An excessively large soil domain can lead to an excessive number of elements and a substantial increase in computational cost. Conversely, a too-small soil domain may fail to effectively mitigate the seismic impact of reflected waves on the structure. According to the research by Lou Menglin^[13], when the total size of the soil domain reaches five times that of the structure, the influence of the lateral boundary on the seismic response of the structure can be neglected, ensuring the accuracy of the FEM results. In this study, a soil calculation width of 135 meters and a selected depth of 60 meters were adopted as the bedrock surface.

The constitutive model of the soil is the Mohr Coulomb model. According to the survey report, the soil layer at the original site has been homogenized. After treatment, the soil density is 1964Kg/m^3 , the elastic modulus is 249MPa , the Poisson's ratio is 0.3, the internal friction angle is 13.76° , and the cohesion is 32.26Kpa ; The concrete grade is C40, using the plastic damage model (CDP), with a density of 2400Kg/m^3 , an elastic modulus of $3.25 \times 10^4\text{MPa}$, and a Poisson's ratio of 0.2. The plastic model is used for

steel reinforcement and steel plate, with an elastic modulus of $2.06 \times 10^5 \text{MPa}$, Poisson's ratio of 0.3, and yield stress of 345MPa.

The element types utilized are C3D8R for soil and concrete, S4R for steel plates, and T3D2 for reinforcing steel bars. According to the research conducted by Du Xiuli^[14], under the precision requirements of numerical simulation, the grid size of soil can be determined using the following formula:

$$h \leq \left(\frac{1}{4} - \frac{1}{8} \right) \lambda \quad (1)$$

In the formula, h represents the grid size of soil, and λ represents the wavelength of the seismic wave. Based on this, the final determination is made the approximate element size for the soil mass as a whole is 2.5m, as shown in Figure 2(a). At the intersection of underground silos, the approximate element size is 1m. For the bottom and top sections of the underground silos, the approximate element size is also 1m. The silo walls are the focus of this study, and the mesh is refined with an approximate element size of 0.5m, as illustrated in Figure 2(b).

The interaction between soil and structures is set as surface-to-surface contact, with a hard contact in the normal direction and a tangential friction coefficient of 0.4. The underground silo is cast-in-situ as a whole, and the various concrete components are bound together using "Tie" constraints. In practice, the concrete and lining steel plates are connected using studs, and their relative displacement is not considered; thus, "Tie" constraints are also used for this connection. The reinforcing steel bars are embedded within the concrete using the "Embedded Region" feature.

In seismic research on underground structures, the viscoelastic boundary, which is currently widely used, can effectively address the issue of simplifying an infinite half-space into a finite computational domain. The viscoelastic artificial boundary can be expressed as a continuously distributed and mutually coupled energy-dissipating spring-damper system. The stiffness and damping coefficients of the normal and tangential springs on the presumed artificial boundary can be determined using specific formulas^[15].

$$K_{BT} = \alpha_T \frac{G}{R}, C_{BT} = \rho c_T \quad (2)$$

$$K_{BN} = \alpha_N \frac{G}{R}, C_{BN} = \rho c_N \quad (3)$$

The formulas are as follows, where K_{BT}, K_{BN} represents the tangential and normal spring coefficients, C_{BT}, C_{BN} represents the tangential and normal damping coefficients, R is the distance from the scattering wave source to the boundary, α_T, α_N is a correction coefficient, recommends values of 0.5 and 1.0. Ma Shengjie's research^[16] indicates that displacement input and acceleration input are only suitable for far-field boundaries and are not applicable to viscoelastic boundaries. Forced acceleration and displacement can render the viscoelastic boundary ineffective, leading to deviations in

the calculation results. When using a viscoelastic boundary, it is advisable to input ground motions using equivalent node forces.

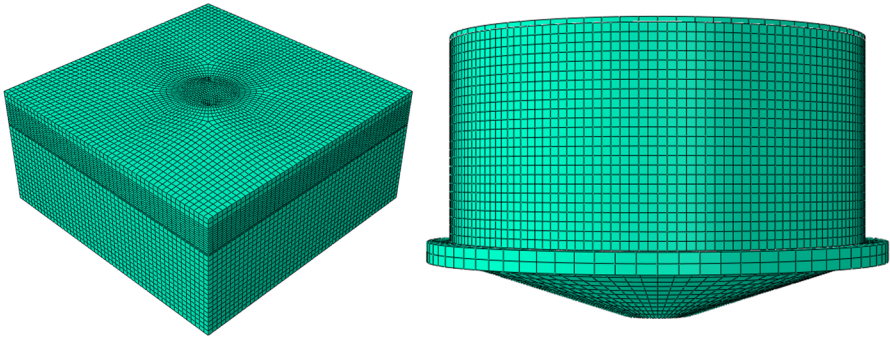


Fig. 2. Mesh division.

2.3 Modal Mode Analysis

Modal analysis is a structural dynamics analysis technique primarily used to determine the natural vibration characteristics of a structure, including modal frequencies, modal damping, and modal shapes. These characteristics form the basis of a structure's response when subjected to dynamic loading. The first six modal frequencies and mode shape characteristics obtained from the modal analysis of the soil-underground silo structure are presented in Table 1.

Table 1. Characteristics of the vibration type.

The amplitude of the order	The vibration type description	Frequency (Hz)	Period (s)
1	Model transverse vibration	0.738	1.35
2	Model vertical vibration	0.739	1.35
3	Rolling vibration in the middle of the model	0.761	1.31
4	Model with a longitudinal and clockwise torsion	0.899	1.11
5	The model rotates counterclockwise horizontally	0.932	1.07
6	The model rotates clockwise horizontally	0.932	1.07

The dynamic response of the structural system is greatly affected by the damping. In this study, the classical ray damping is selected to reflect the energy consumption characteristics of the structure. The damping expression is:

$$C = \alpha[M] + \beta[K] \quad (4)$$

In the formula, α , β represents the Rayleigh damping constant, M represents the overall mass matrix, and K represents the overall stiffness matrix.

The damping constant can be calculated by the following equation:

$$\alpha = 2\zeta \frac{\omega_a \omega_b}{\omega_a + \omega_b} \quad \beta = 2\zeta \frac{1}{\omega_a + \omega_b} \quad (5)$$

In the formula, ω_a , ω_b represents the natural circular frequencies of the structure at order a and b.

The recommended soil damping ratio in the *Code for Seismic Safety Evaluation of Engineering Sites* is $\zeta = 0.05$. Calculated as $\alpha = 0.23$, $\beta = 0.01$.

3 Analysis of Dynamic Characteristics of Underground Warehouses

For underground structures, the direction of incident seismic waves has a significant impact on their dynamic response characteristics. Although numerous studies have highlighted the prominent influence of horizontal seismic waves on underground structures, to comprehensively investigate the response characteristics of underground silos under seismic actions, it is necessary to simulate the seismic response of these structures to horizontal seismic waves, vertical seismic waves, and coupled horizontal-vertical seismic waves. Observations from existing data reveal that the peak acceleration of vertical seismic waves is generally lower than that of horizontal seismic waves, typically accounting for approximately two-thirds of the horizontal seismic wave's peak acceleration. In this section, the Imperial Valley-06 wave is selected as the input excitation wave, with its acceleration time-history curve shown in Figure 3.

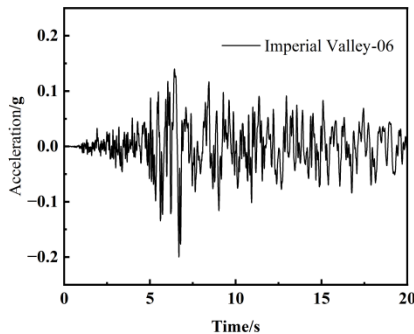


Fig. 3. The Imperial Valley-06 wave.

This study considers the influence of unidirectional and bidirectional input of the Imperial Valley-06 wave on the dynamic response of the walls of the underground silo. The peak horizontal acceleration of the input Imperial Valley-06 wave is 0.3g, and the peak vertical acceleration is 0.2g. The analysis conditions are shown in Table 2. Four measurement points are arranged circumferentially every 90° at the top and bottom of the silo wall, and 13 measurement points are arranged vertically (along the buried depth of the silo wall). The arrangement of measurement points is illustrated in Figure 4.

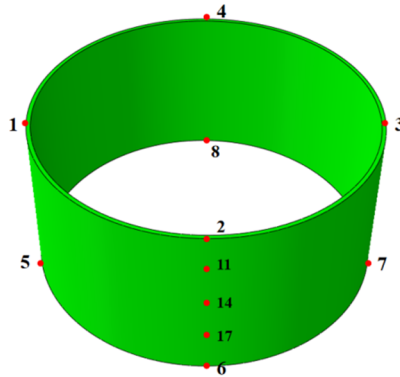


Fig. 4. Layout of the monitoring points.

Table 2. Three analysis working conditions.

Operating mode	Peak acceleration	Mode of action of the ground motion
1	0.3	Horizontal
2	0.2	Vertical
3	0.3+0.2	Horizontal + Vertical

3.1 Acceleration Response Analysis

Table 3 presents the absolute peak acceleration values at various monitoring points under different working conditions. From Table 3, it can be observed that under the action of seismic waves, the acceleration response at the top of the silo wall is higher than that at the bottom, with a more pronounced effect under horizontal seismic waves. The acceleration response is basically the same at the same height. A graph depicting the variation of peak acceleration along the buried depth of the silo wall is shown in Figure 5. Under the action of seismic waves incident from different directions, the peak acceleration of the silo wall decreases overall with increasing buried depth. The horizontal acceleration increases significantly, while the vertical acceleration increases slightly. Under coupled seismic action, both the horizontal and vertical accelerations of the silo wall increase compared to those under unidirectional seismic action. The maximum horizontal accelerations of the silo wall under horizontal seismic action and coupled seismic action are 2.419 m/s² and 2.571 m/s², respectively, with an increase of approximately 6%. The maximum vertical accelerations of the silo wall under vertical seismic action and coupled seismic action are 2.162 m/s² and 2.465 m/s², respectively, with an increase in vertical acceleration of approximately 12%. Therefore, compared to considering only unidirectional seismic action, the response of the silo wall is greater under coupled seismic action, with a more significant impact on vertical seismic effects. Under the action of coupled seismic waves, the low-order vibration modes (such as the first-order bending and torsion) of the silo structure can produce superimposed resonance with higher-order vibration modes. Compared to considering only unidirectional

tional seismic effects, the silo wall exhibits a more significant response under coupled ground motions, and there is a greater impact on vertical seismic effects.

Table 3. Peak acceleration at the monitoring points.

Monitoring site	Case 1 Horizontal peak acceleration (m/s ²)	Case 3 Horizontal peak acceleration (m/s ²)	Case 2 Vertical peak acceleration (m/s ²)	Case 3 Vertical peak acceleration (m/s ²)
1	2.419	2.559	2.162	2.414
2	2.381	2.563	2.153	2.365
3	2.469	2.665	2.155	2.416
4	2.383	2.271	2.148	2.386
5	2.051	2.064	2.139	2.386
6	2.049	2.190	2.138	2.277
7	2.033	2.179	2.140	2.297
8	2.074	2.186	2.139	2.281

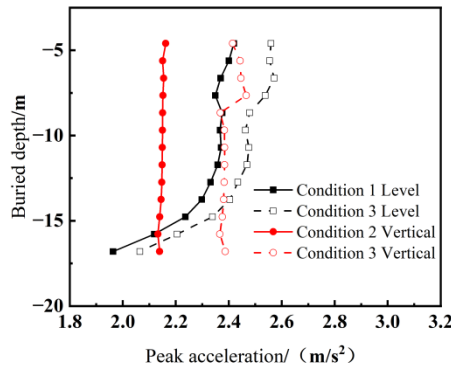
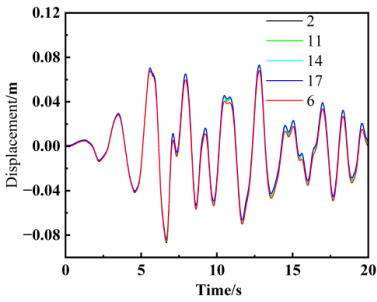


Fig. 5. Changes in the peak acceleration.

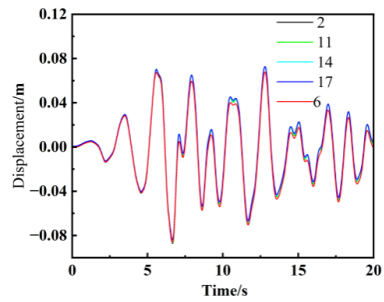
3.2 Analysis of the Shift Reactions

Figure 6 shows the horizontal displacement time-history curves of points 2, 11, 14, 17, and 6 along the buried depth direction of the silo wall under horizontal and coupled seismic actions. The displacements at each monitoring point are basically the same, indicating good integrity of the silo wall. The peak horizontal displacements occur at 6.66s, with peak displacements of 8.68mm and 8.71mm, respectively. The relative displacement between the top of the silo wall (point 2) and the bottom (point 6) is not the largest; instead, the largest relative displacement occurs between points 17 and 6, indicating that the largest relative displacement is within the bottom one-third of the silo wall. Figure 7 presents the relative displacement time-history curve between these two points. Under seismic action, the relative displacement between points 17 and 6 is overall larger, with the maximum relative displacement occurring at 7.06s. The maximum relative displacement between points 17 and 6 under both seismic actions is

6.6mm, and the maximum relative displacement between the top and bottom of the silo wall under coupled seismic action is 7.07mm.

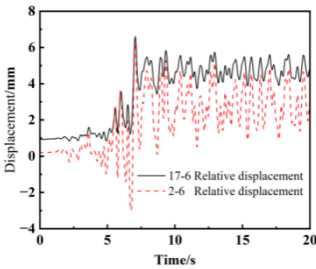


(a) Horizontal displacement time history curve of working condition 1

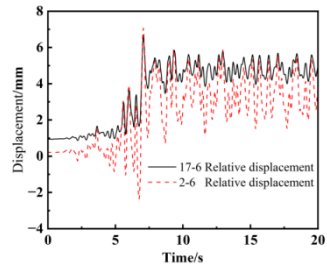


(b) Horizontal displacement time history curve of working condition 3

Fig. 6. Horizontal displacement time course curve



(a) Horizontal relative displacement time history curve of working condition 1



(b) Horizontal relative displacement time history curve of working condition 3

Fig. 7. The horizontal relative displacement time course curve

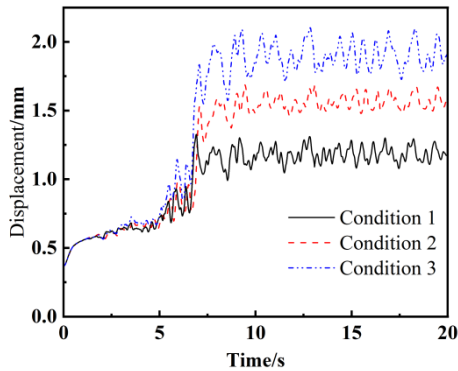


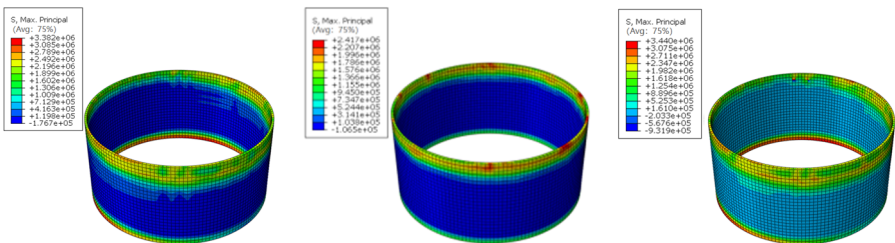
Fig. 8. Vertical relative displacement curves of the top and bottom of the silo walls

The vertical relative displacement time-history curve between the top and bottom of the underground silo wall (points 2 and 6) is shown in Figure 8. The vertical deformation of the silo wall is basically consistent under seismic waves incident from different directions. The relative displacement increases sharply at the peak of the seismic wave and then tends to stabilize with slight fluctuations. The residual deformations for working conditions 1, 2, and 3 are 1.17mm, 1.58mm, and 1.90mm, respectively.

3.3 Stress Response Analysis

The stress contour plot provides an intuitive representation of the stress distribution in the silo wall under seismic action, as shown in Figure 9. The silo wall employs the Concrete Damaged Plasticity (CDP) model, where concrete failure is controlled by its first and third principal stresses. Concrete undergoes plastic failure when the ratio of the first principal stress to the third principal stress exceeds the ratio of the tensile strength standard value to the compressive strength standard value. The figure displays the contour plots of the first principal stress (S-MAX-Princip) and the third principal stress (S-MIN-Principa) at the moment of maximum relative displacement between the top and bottom of the silo wall. As shown in Figure 9, the maximum first principal stresses on the silo walls for working conditions 1, 2, and 3 are 3.382 MPa, 2.417 MPa, and 3.440 MPa, respectively, all exceeding the ultimate tensile strength capacity of concrete, which is 2.39 MPa. Under vertical seismic action, the tensile stress in the concrete at the top of the silo wall is relatively small. The maximum third principal stresses on the silo walls for working conditions 1, 2, and 3 are 5.240 MPa, 3.321 MPa, and 5.277 MPa, respectively, all exceeding the ultimate compressive strength capacity of concrete, which is noted as 26.8 MPa but appears to be a typographical error considering typical concrete compressive strengths; for the sake of this translation, we assume it should be a much lower value relevant to tensile strength for comparison context, but retain the original number for accuracy.

The upper one-eighth and the bottom of the silo wall experience significant tensile forces. Acceleration analysis reveals that the upper part of the silo wall experiences the maximum acceleration and displacement, potentially leading to plastic failure and the development of cracks in this region. The relative displacement between the lower one-third of the silo wall and its base is large, with a significant increase in horizontal acceleration in this area, resulting in the maximum compressive stress on the silo wall at this location.



(a) Condition 1 First principal stress (b) Condition 2 First principal stress (c) Condition 3 First principal stress

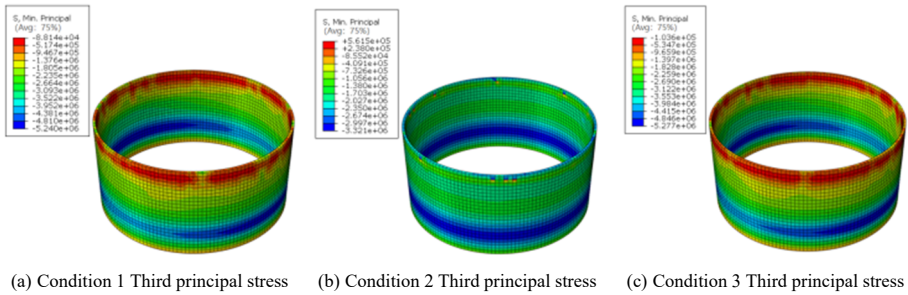


Fig. 9. Cloud diagram of warehouse wall stress

4 Conclusion

This study established a soil-underground grain silo interaction model using the finite element software ABAQUS to simulate the response of underground grain silos under seismic loading and to investigate the stress and deformation of the silo wall under seismic loads from different incident directions. The following conclusions were drawn: (1) The underground silo wall exhibits different responses to seismic waves from different incident directions. The influence of horizontal seismic waves on the silo wall is greater than that of vertical seismic waves. Coupled seismic action amplifies the acceleration, displacement, and stress responses of the silo wall. (2) The acceleration of the silo wall decreases as the burial depth increases. The horizontal relative displacement is larger at the location one-third from the bottom of the silo wall and at the base of the wall. Both the tensile stresses at the top one-eighth and the bottom of the silo wall under horizontal seismic action exceed the standard value of ultimate tensile strength. Therefore, during the design phase, it is recommended to increase the reinforcement ratio or enhance the reinforcement strength.

References

1. Chen Y, Qiu G P, Zhang R Y, et al.(2023) Experiment and Simulation Research of Different Lining Materials for Underground Granary [J]. *Journal of Solar Energy*, 44(06):53-60
2. Wang Z Q, Chuai J, Liu Y C, et al.(2019) Current Situation and New Progresses of Structure Design of Underground Silos[J]. *Journal of Henan University of Technology (Natural Science edition)*,40(05):132-138.
3. Du X L, Pan Y C, Zhao M, et al. (2023)Comparative Study on Seismic Performance of Underground Station Structure with Different New Functional Columns[J]. *Project seismic and reinforcement renovation*, 45(03):91-101
4. Gao X. (2024)Lateral Seismic Response of Immersed Tube Tunnel based on Time History Analysis Method [J]. *Cryogenic Building Technology*, 46(08):86-89.
5. Wu Q, Ding X, Zhang Y, et al.(2024) Experimental and numerical study on dynamic response of underground structure in coral sand under earthquakes[J]. *Journal of Earthquake Engineering*, 28(1): 62-84.

6. Han G H, Su C. (2022)Analysis of Seismic Response of Underground Cavern Based on Viscoelastic Boundary[J]. *Hydropower and Energy Science*, 40(10):135-139+199.
7. Liu D, Du X, El Naggar H M, et al.(2022)Seismic mitigation performance analysis of underground subway station with arc grooved roller bearings[J]. *Soil Dynamics and Earthquake Engineering*, 153: 107082.
8. Xu M Z, Cui Z D, Yuan L..(2024)Effect of different groundwater levels on seismic response of subway stations shallowly buried in the sand foundation[J]. *Geomechanics and Engineering*,39(3): 317.
9. Huang W Z, He C, Xu G Y, et al. (2024)Seismic Response of a Submarine Immersed Tunnel Under Oblique Incidence of SV Waves[J]. *Tunnel construction (Chinese and English)*, 44 (04): 724-738.
10. Gu K S, Zhou J, Dai F C, et al. (2024)Dynamic Response Analysis of Single Slope Under Oblique Incidence of Seismic P Wave [J]. *Journal of Geophysics*,67 (06): 2350-2363.
11. Cui Z D, Yan W X, Wang S Y. (2024)Collapse failure mechanism of subway station under mainshock-aftershocks in the soft area[J]. *Geomechanics and Engineering*, 36(3): 303-316.
12. Zhu H, Yan S H, Sun W Y, et al.(2024) Seismic Response Analysis of Shallow-Buried Unsymmetrical-Loading Double Tunnel Under Oblique Incidence of Seismic Wave [J]. *vibrate. Test and Diagnosis*, 44(02):259-265+407.
13. Lou M L, Pan D G, Fan L C. (2003)Effect of Vertical Artificial Boundary on Seismic Response of Soil Layer[J]. *Journal of Tongji University (Natural Science Edition)*, (07): 757-761.
14. Du X L, et al. (2017)Collapse Simulation and Failure Mechanism Analysis of the Daikai Subway Station Under Seismic Loads[J]. *China Civil Engineering Journal*,50(01):53-62+69.
15. Chi H, Wang S S, Wang W. (2022)Application of Viscoelastic Artificial Boundary in Seismic Analysis of Underground Structures[J]. *Urban Roads Bridges and Flood Control*,(01):237-241+27.
16. Ma S J, et al. (2020)Implementation of Viscous-spring Boundary in ABAQUS and Comparativestudy on Seismic Motion Input Methods[J]. *Chinese Journal of Rock Mechanics and Engineering*,39(07):1445-1457.

Open Access This chapter is licensed under the terms of the Creative Commons Attribution-NonCommercial 4.0 International License (<http://creativecommons.org/licenses/by-nc/4.0/>), which permits any noncommercial use, sharing, adaptation, distribution and reproduction in any medium or format, as long as you give appropriate credit to the original author(s) and the source, provide a link to the Creative Commons license and indicate if changes were made.

The images or other third party material in this chapter are included in the chapter's Creative Commons license, unless indicated otherwise in a credit line to the material. If material is not included in the chapter's Creative Commons license and your intended use is not permitted by statutory regulation or exceeds the permitted use, you will need to obtain permission directly from the copyright holder.

